AIAA SciTech Forum
6-10 January 2025, Orlando, FL
AIAA SCITECH 2025 Forum

10.2514/6.2025-2123

Flow Visualization of Liquid Nitrogen Flow Boiling in Horizontal Heated Tubes

Sunjae Kim[1],
Purdue University, West Lafayette, IN, 47096

Jason Hartwig[2],
NASA Glenn Research Center, Cleveland, OH, 44135

Nishad Damle[3], Dylan Foster[4], Steve Darges[5], Issam Mudawar[6],
Purdue University, West Lafayette, IN, 47096

NASA and Purdue University have been collaborating on addressing various aspects of flow boiling for nearly two decades. Understanding the flow conditions and flow patterns over which the onset of nucleate boiling or critical heat flux occurs allows designers to set limits on the allowable heat flux into the transfer line to prevent or limit boiling. This paper presents detailed flow visualization of recently conducted liquid nitrogen flow boiling experiments in heated tubes in the horizontal flow configuration. High-speed video recordings through a sight glass were utilized to capture two-phase flow patterns and interfacial behaviors as a function of different mass flux and heat flux. At low mass flux, the dominant flow patterns include bubbly, plug, slug, stratified annular, and annular flows. At higher mass flux, the dominant flow pattern tends towards a uniform bubbly flow due to stronger flow inertia. As heat flux is increased, the flow generally transitions into annular flow.

I. Introduction

Future in-space cryogenic propulsion systems will likely be required to facilitate future missions beyond Low Earth Orbit. These systems include ascent and descent chemical propulsion stages [1], fuel depots [2], and advanced concepts such as nuclear thermal propulsion [3] and nuclear electric propulsion [4]. Compared to storable propulsion systems, cryogenic propulsion systems offer higher performance in terms of specific impulse, and safety and environmental benefits.

Cryogens are fluids that exist as gases at room temperature. As such, difficulties arise when storing and transferring cryogenic propellants. For example, the low normal boiling point of cryogens and low superheat required to initiate boiling leads to high heat transfer rates between environment and fluid, and high susceptibility to boiling and two-phase flow. Cryogens have low surface tension and low latent heat of vaporization, which also leads to higher susceptibility to boiling due to smaller bubbles nucleating and detaching from heated surfaces.

[1]Graduate Assistant, Boiling and Two-Phase Flow Laboratory, School of Mechanical Engineering, Mechanical Engineering Building, 585 Purdue Mall, West Lafayette, IN 47907
[2]Research Aerospace Engineer, Fluids and Cryogenics Branch, 21000 Brookpark Road, Cleveland, OH, 44135, AIAA Associate Fellow.
[3]Graduate Assistant, Boiling and Two-Phase Flow Laboratory, School of Mechanical Engineering, Mechanical Engineering Building, 585 Purdue Mall, West Lafayette, IN 47907
[4]Graduate Assistant, Boiling and Two-Phase Flow Laboratory, School of Mechanical Engineering, Mechanical Engineering Building, 585 Purdue Mall, West Lafayette, IN 47907
[5]Graduate Assistant, Boiling and Two-Phase Flow Laboratory, School of Mechanical Engineering, Mechanical Engineering Building, 585 Purdue Mall, West Lafayette, IN 47907
[6]Betty Ruth and Milton B. Hollander Family Professor of Mechanical Engineering, School of Mechanical Engineering, Mechanical Engineering Building, 585 Purdue Mall, West Lafayette, IN 47907, AIAA Senior Member

For most envisioned cases of in-space cryogenic propellant transfer in missions beyond Low Earth Orbit, it is highly desirable to transfer single-phase or near-single phase liquid flow. For engines, single-phase flow is desired to avoid combustion instability in the engine. For cryogenic fuel depots, single-phase flow is desired to avoid cavitation in pumps and valves, and to ensure high final liquid volume fraction in the receiver tank. During propellant transfer, it is essential to ensure the system hardware be chilled down to the fluid saturation temperature as quickly and efficiently as possible. This chilldown process is generally accomplished through boiling heat transfer between cold cryogen and warm transfer hardware. Afterwards, it is desired to maintain the system at or below cryogenic temperatures. For steady state transfer system operation, the subcooled margin of the liquid in the propellant storage tank should be sufficiently high to overcome the parasitic heat leak into the transfer system such that single-phase or near-single phase liquid is achievable at the exit. The emphasis of the current work is to characterize the behavior of this steady state cryogenic flow boiling phenomena.

The purpose of this paper is to present detailed flow visualization results for recently conducted liquid nitrogen (LN_2) flow boiling experiments in the horizontal flow orientation under terrestrial gravity conditions. This paper is intended to introduce how various operating parameters affect the two-phase heat transfer process and observed two phase flow patterns. The primary parameters that are varied in the current study include mass flux and heat flux. The outline of the paper is as follows: first a summary is presented on flow boiling physics and previous related flow boiling experiments which included flow visualization. Next, the description of the experimental system is given, along with the flow visualization test section, and experimental methodology for conducting experiments. Next, flow boiling curves and detailed images of the flow visualization are presented as a function of mass flux and heat flux to explain trends in the data. Finally, the conclusion section summarizes key findings.

II. Background

A. Flow Boiling Physics

Heat transfer of any boiling liquid can be described through a boiling curve, which plots the wall heat flux against the wall superheat (temperature difference between the tube inner wall and the fluid saturation temperature). Figure 1 plots the boiling curve for saturated water from [4]. The steady state heating configuration of the boiling curve is shown with red arrows from left to right and the quenching (or chilldown) configuration with black arrows is shown from right to left. In the quenching case, the tube wall temperature begins significantly above the fluid saturation temperature, and the cold fluid quenches the tube until the boiling subsides and single-phase liquid flow ensues. In the steady state heating case, the subject of the current work, single-phase liquid flow is already established, and an external heat source gradually boils the liquid. Initially, single-phase liquid heat transfer is prevalent. As wall heat flux is increased, wall superheat begins to increase, and bubbles begin to form following the onset of nucleate boiling (ONB). Nucleate boiling is then encountered, characterized by the presence of isolated bubbles. The bubble nucleation, departure, and liquid replenishment induce mixing near the surface, increasing the allowable wall heat flux and the ensuing heat transfer coefficient (HTC). In nucleate boiling, heat transfer is generally dominated by latent heat of vaporization. As wall heat flux further increases, nucleate boiling is suppressed and convective boiling ensues. Eventually, the critical heat flux (CHF) point is reached, signaling the maximum allowable heat removal rate in two-phase boiling flow. Beyond CHF, a vapor blanket is formed along the wall characteristic of film boiling, preventing liquid from wetting the surface, leading to a rapid rise in wall superheat. Operationally, this regime is called thermal runaway, and may be dangerous due to a combination of high heat flux, poor heat transfer through the insulating vapor blanket, and high ensuing wall temperatures. Eventually, the liquid film vaporizes where the flow generally proceeds from annular flow to dispersed flow and eventually to single-phase vapor flow. The focus in the current work is on characterizing cryogenic nucleate flow boiling heat transfer in the heating configuration.

For flow boiling tests in the heating configuration, heat flux is the control variable and wall superheat is the response variable. Tests begin with the wall and fluid at the same temperature and power is delivered in a series of small increments to the test section typically through an electrical coil. Data is usually acquired at steady-state conditions for fixed values of heat flux. Because the imposed heat flux is generally one or two orders of magnitude higher than the parasitic heat leak, uncertainties are typically low for extracting HTCs from steady state heating over quenching experiments.

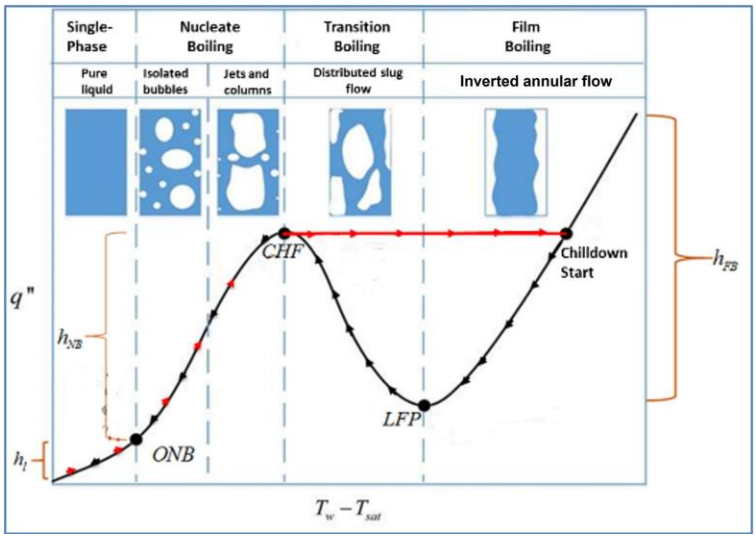

Figure 1: Boiling Curve Illustrating Heating and Quenching Configurations

B. Previous Flow Boiling Visualization Studies

As mentioned in several recent articles [6-9], cryogenic flow boiling experiments have been conducted for several decades. However, only recently have studies been performed with the necessary high instrumentation density, flow visualization, and systematic, parametric analysis of preponderant variables that affect performance. In collaboration with NASA Glenn Research Center, a new cryogenic flow boiling facility has been designed, built, and tested at Purdue University, successfully filling several gaps in the world consolidated cryogenic flow boiling database. The data has been used to systematically understand the impacts of various operational parameters on cryogenic flow boiling in heated tubes [10, 11]. The data can be also used to assess or develop fundamental correlations or subroutines used to assist in designing future cryogenic propellant transfer systems.

While some visualization studies have been performed for cryogenic boiling in the quenching configuration [12-17], where the focus is predominately on film boiling, detailed flow visualization is generally missing from cryogenic flow boiling experiments in the heating configuration. To the authors' knowledge, there are three reported studies. First, the earliest known report of cryogenic two-phase flow boiling visualization is from Simoneau and Simon [18]. Here, a series of two-phase flow images were presented to compare vertical upflow to vertical downflow. The authors showed images indicating higher vapor accumulation in vertical downflow versus upflow that were correlated to the lower CHF for downflow versus upflow. Second, Van Dresar [19] reported some flow images of liquid hydrogen and LN_2 flow boiling in tubes at low mass flux. Third, Fu et al. [25] studied microchannel flow patterns for LN_2 steady-state flow boiling in the vertical upflow orientation. Despite their efforts, the flow patterns do not represent the macro-channel flow boiling of cryogens in tube sizes relevant for most future applications. The LN_2 flow boiling flow visualization in the current work builds upon historical results by providing detailed imagery at multiple different mass fluxes and heat fluxes in a macro-channel tube.

III. Experimental Description

A. Facility and Flow Visualization Test Section

A detailed description of the new Purdue University cryogenic flow boiling facility, test section, and instrumentation are available in Kim et al. [10, 11]; only a brief description is given here. Figure 2 shows the computer aided drawing (CAD) of the facility and Figure 3 shows the CAD of the flow visualization test section. For ground testing, a gaseous nitrogen cylinder was used to pressurize and expel the LN_2 from a 160-liter vacuum jacketed stainless steel (SS) supply dewar. Liquid is routed through a turbine flow meter used to measure volumetric flow rate at high mass flux. Liquid is then routed through the heated tube test section chamber, which housed the 8.5 mm inner diameter, 0.5 mm wall-thickness 304SS heated tube. Up to 3200 W of heat could be supplied to the tube. Immediately downstream, the flow was then routed through the flow visualization test section chamber, which housed a Pyrex sight glass. A high-speed camera was used to observe the evolving two-phase flow patterns. Vacuum pumps were used to pump down the pressure in both chambers to ~0.1 Pa in order to reduce the parasitic heat leak.

Downstream of both test sections was a needle valve used to precisely control mass flux. Flow was then routed through the vent heater assembly, a series of 3 kW heaters to vaporize any remaining liquid before venting overboard. Downstream of the heaters were two flow lines, one with a vapor flow meter used to measure low mass fluxes (< G = 100 kg/m^{2}s). After the two lines merged, there was a separator tank as shown in Figure 2 that was used to trap any non-vaporized liquid.

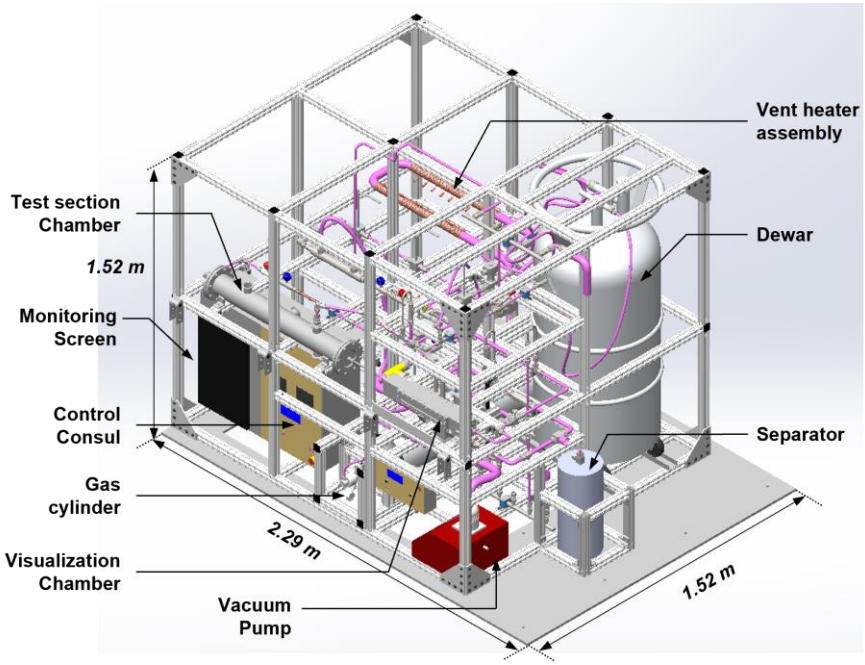

Figure 2: Cryogenic Flow Boiling Test Facility

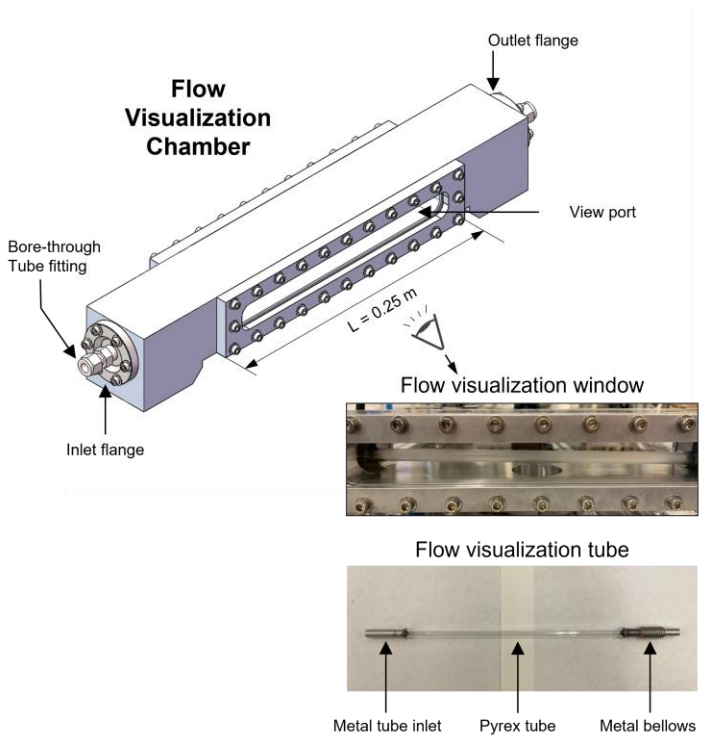

Figure 3: Flow Visualization Sight Glass Chamber and Test Section

The visualization chamber was a vacuum chamber that housed the Pyrex sight glass. The chamber was comprised of a rectangular SS housing with inlet and outlet flanges for both ends to ensure vacuum-tight sealing. Transparent glass windows were attached to each side, providing a visualization length of 0.25 m. On one side, the high-speed camera was mounted to record videos, while the other side was used for illumination. The Pyrex tube had a metal bellows attached to one end, similar to what was used in previous LH_2 line chilldown flow visualization [16, 17] to reduce thermal stresses. The outer diameter of the tube was 9.5 mm, while the inner diameter was approximately equal to the inner diameter of the heated tube test section of 8.5 mm. This was done to reduce unnecessary flow disturbances. The length of the visualization tube was slightly longer than 0.25 m such that the entire flow section could be visualized. The test section and visualization chambers were connected by adjoining the tubing, which was then connected to a vacuum hose with a butterfly valve in between to isolate the vacuum line when needed.

Pertinent instrumentation for the cryogenic flow boiling rig is as follows: a turbine flow meter was used to measure liquid flow rate upstream of the test sections and a gas flow meter was used to measure flow rate downstream. Stream temperature and pressure were measured upstream of the heated tube test section, upstream of the flow visualization test section, and upstream of the vent heater assembly to determine the thermodynamic state of the fluid. Vacuum pressure was measured for both test section chambers. 14 thermocouples were attached to the heated tube test section, one mounted at the top and one at the bottom at each of 7 axial locations. The electrical power supplied to the heated tube was measured by a power meter.

As shown in Figure 2, a control consul and screen were mounted on the bottom left corner of the rig and were used to log and monitor all sensor output signals. Data was measured at 80 Hz nominally. The control consul also contained the data logger, AC power distributors, DC power converter, circuit breakers, heater power controllers for test section heaters, heater temperature controllers for vent heaters, power meters for each heater, and an Arduino board for pressure control.

B. Experimental Methodology

The following procedure was used to run a typical heated tube test: to begin a test, the LN_2 supply tank was pressurized to the desired target pressure. Main flow system valves were all operated in open loop configuration, the dewar was then opened to chill down the entire system hardware, and the vent heaters were activated. During chilldown, the thermodynamic state of the fluid was monitored at the various pressure/temperature stations, and the fluid was visualized in the sight glass. After sufficient chilldown time, the inlet state to the test section was confirmed to be subcooled liquid, signaling the start of a controlled experiment. Tests were then performed by increasing heat flux with small increments until the system reached CHF for different inlet subcooling, pressure, and mass flux. Tests were generally run at fixed flow rates, pressures, and inlet subcooling. The dewar pressure was adjusted to influence the test section pressure, and the needle valve was used to dial in the precise flow rate. Heat flux was then adjusted at fixed values, and all control variables were allowed to reach steady state. As higher heat fluxes were set, the wall temperature slowly climbed as nucleate boiling increased. Finer adjustments in heat flux were made as the system approached the CHF. At the point of CHF, the wall temperature exhibited unsteady excursions, after which heater power was cut off to avoid thermal runaway. Once liquid in the supply dewar was sufficiently drained, testing was completed.

IV. Results and Discussion

A. Heat Transfer Coefficient

Numerous LN_2 flow boiling experiments were conducted to examine the effect of pressure, inlet subcooling, equilibrium quality, mass flux, heat flux, and flow orientation. Results in the current work are for horizontal flow boiling experiments, with a focus on the effect of mass flux and heat flux. First, boiling curves are analyzed, then the flow visualization test section images.

Figure 4 shows a summary of these results, where LN_2 boiling curves are plotted, in terms of the wall heat flux as a function of wall superheat, four different mass fluxes, but at near-constant inlet pressure and inlet subcooling. Top wall temperatures at the 7 different axial locations are averaged, as are the bottom wall temperatures. While tests were conducted with heat flux as the control variable and wall superheat as the response variable, it is instructive to plot the boiling curve as shown. First, for both sensor locations and all mass fluxes tested, there are generally two distinct slopes: a weak slope for single-phase to the ONB, and a much steeper slope for ONB to CHF, characteristic of nucleate boiling heat transfer. This slope change is predominately due to the

contribution and dominance of latent heat transfer over simple forced convection heat transfer. Second, at lower mass fluxes, the differences between top and bottom sensors are more noticeable, but at higher mass flux, the curves approach one another. This is attributed to inertial forces dominating over buoyancy forces. Third, higher mass flux generally leads to higher nucleate boiling heat transfer, and a delay of approaching the CHF, implying that high mass flux can sustain nucleate boiling for larger heat fluxes due to higher efficiency of vapor removal. Fourth and finally, for all mass fluxes tested, higher heat transfer is obtained at the bottom of the tube as opposed to the top of the tube, primarily due to the higher propensity for liquid to remain at the bottom of the tube, thus sweeping away vapor bubbles generated during nucleate boiling.

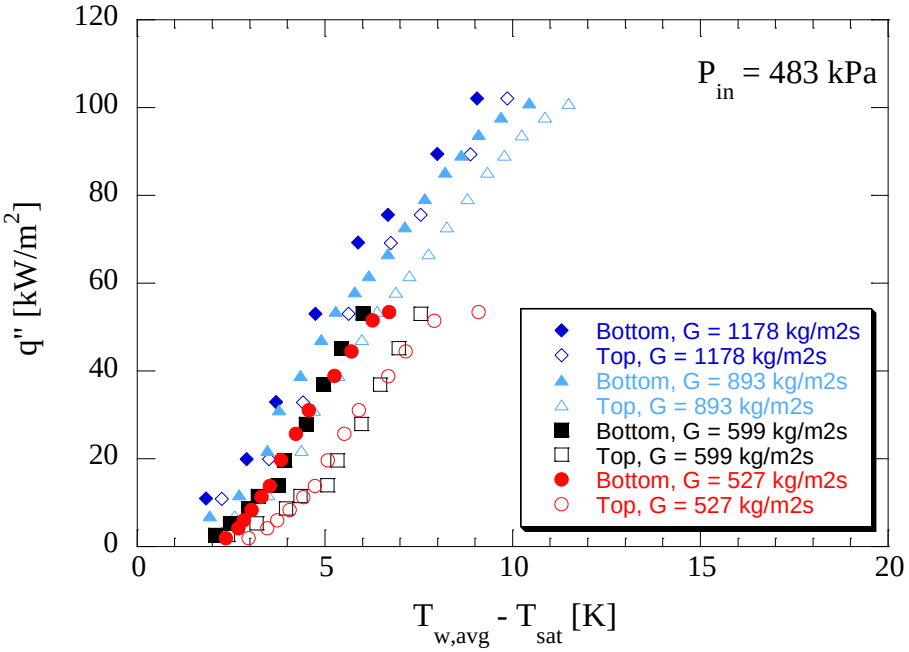

Figure 4: Nucleate Boiling Heat Flux as a Function of Wall Superheat and Mass Flux for Horizontal Flow Tests

B. Flow Visualization Time Sequence, Low Mass Flux

To examine the effect of different heat flux on the flow profiles during nucleate boiling at low mass flux, Figures 5, 6, and 7 plot high-speed image sequences for a mass velocity of G = 561 kg/m^{2}s, P_{in} = 344 kPa, and ΔT_{sub} = 1.68 K at three different wall heat flux conditions, q" of 10%, 19%, and 60% q''_{CHF}, respectively. The images in each sequence are 10 ms apart. At 10% q''_{CHF} in Figure 5, discrete bubbles enter the visualization tube across the entire cross-sectional area of the tube inlet not only through the top portion of the area. The bubbles flowing through the lower half of the tube gradually ascend toward the top surface. As shown in Figure 5 and as indicated with red arrows, a cluster of bubbles flowing into the tube inlet are tracked with the time. With buoyancy effects, small bubbles travel up towards the top surface and accumulate, which can be observed from the first and second images. However, from the second to third image of Figure 5, clustered bubbles suddenly disperse and travel away from each other without being merged. According to Sharma et al. [21], small sized bubbles, when collided or densely packed due to the bubble collision dispersion force, are repelled from each other resulting in well distributed bubble concentrations across the cross-sectional area of the tube. From actual flow visualization in these figures, the diffusion of highly concentrated bubbles after their sudden accumulation is clearly captured. As flow proceeds, due to the overpowering of the body force and reduction of the bubble collision dispersion force effect with increasing bubble diameter, the merging of bubbles takes place and forms a vapor plug. In addition, with the absence of boiling within the visualization tube, the turbulent mixing effect is less apparent than it is in the test section where bubble nucleation and departure are active. Therefore, as bubbles proceed through the visualization section, the interface become less wavy and the variation of flow structure reduces.

At 19% $q''_{CHF,}$ as shown in Figure 6, a larger and elongated vapor structure enters the visualization tube. As shown in Figure 6, plugs are connected due to increasing vapor generation within the test section, covering

almost the entire length of the visualization section. As heat flux increases up to 60% q''_{CHF} as shown in Figure 7, the flow pattern develops into annular flow having an annular liquid film around the vapor core.

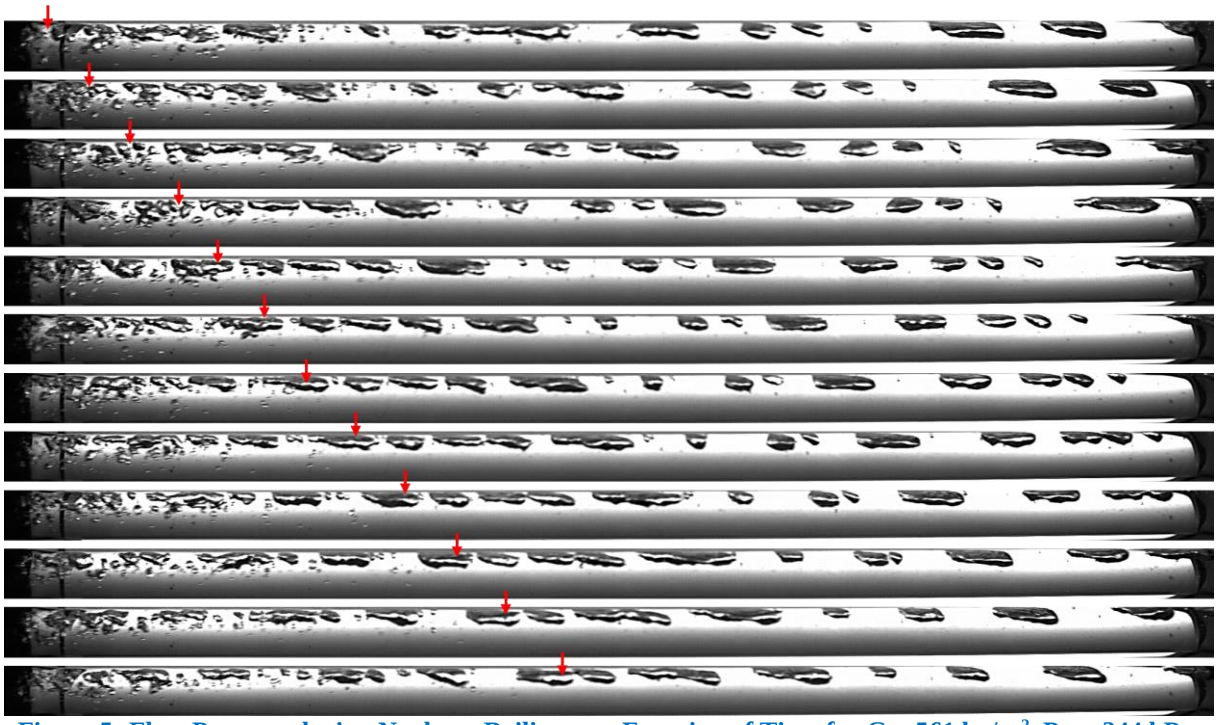

Figure 5: Flow Patterns during Nucleate Boiling as a Function of Time for G = 561 kg/m^2, P_{in} = 344 kPa, $\Delta T_{sub,in}$ = 1.7 K, 10% q"$_{CHF}$, $x_{E,out}$ = -0.005. Images are taken approximately 10 ms apart.

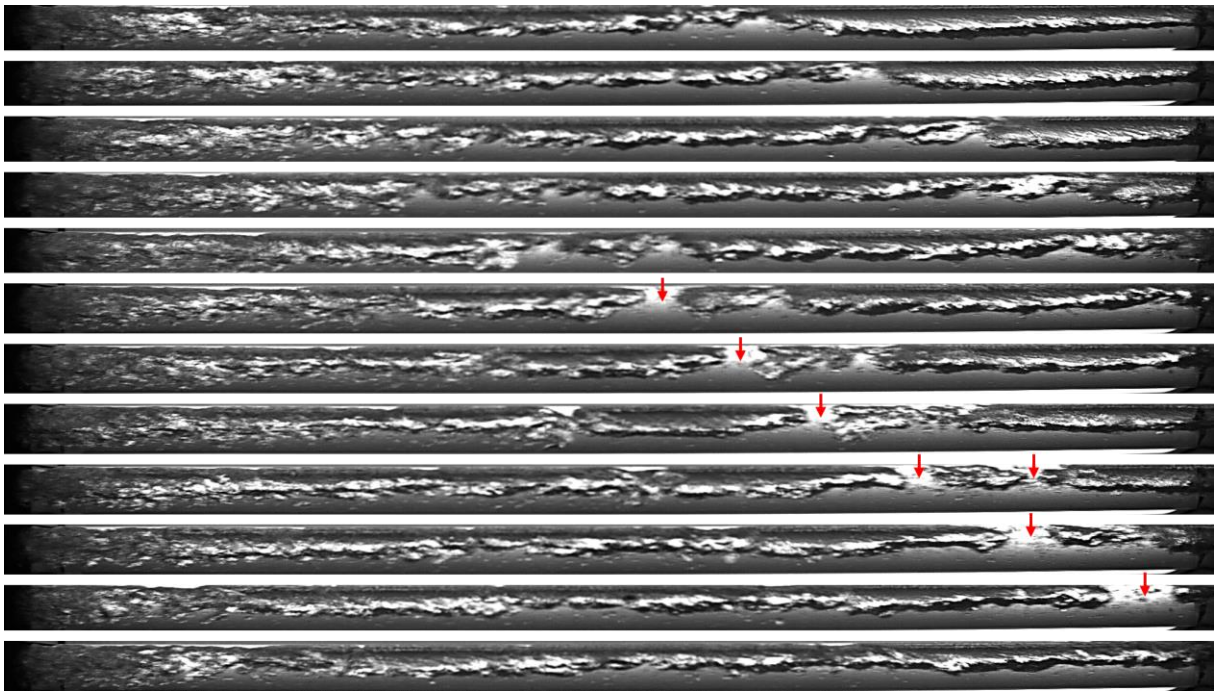

Figure 6: Flow Patterns during Nucleate Boiling as a Function of Time for G = 561 kg/m^2, P_{in} = 344 kPa, $\Delta T_{sub,in}$ = 1.7 K, 19% q"$_{CHF}$, $x_{E,out}$ = 0.02. Images are taken approximately 10 ms apart.

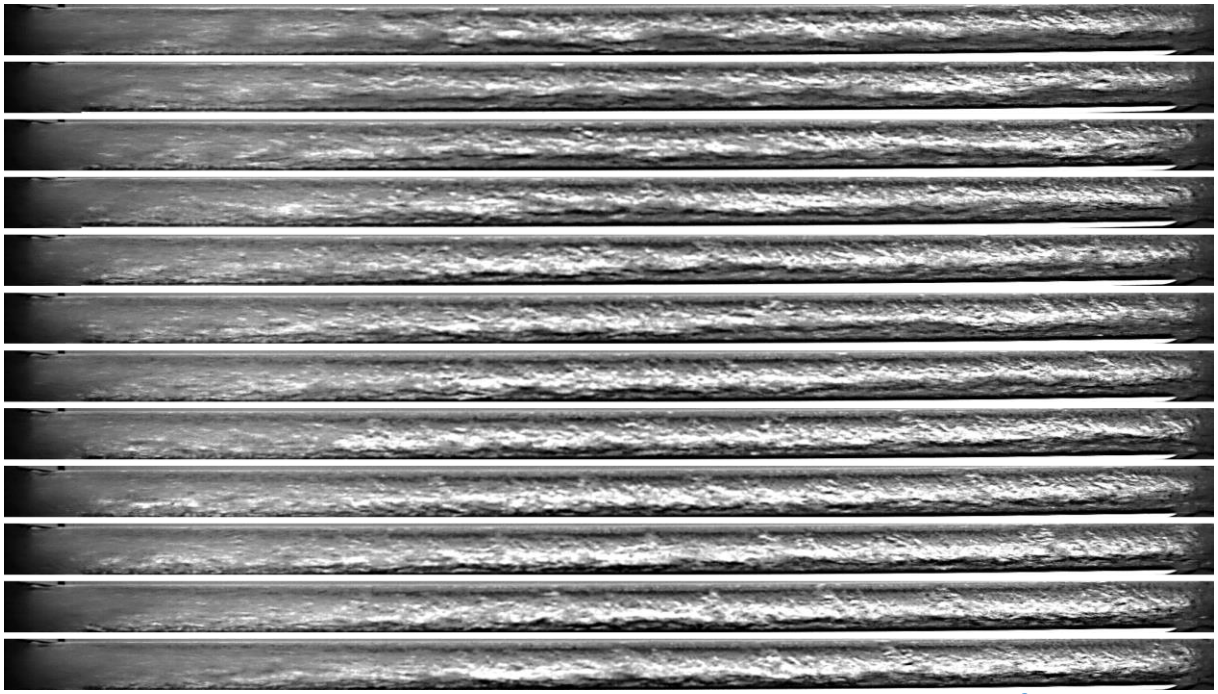

Figure 7: Flow Patterns during Nucleate Boiling as a Function of Time for G = 561 kg/m^2, P_{in} = 344 kPa, $\Delta T_{sub,in}$ = 1.7 K, 60% q"$_{CHF}$, $x_{E,out}$ = 0.02. Images are taken approximately 10 ms apart.

C. Flow Visualization Time Sequence, High Mass Flux

To examine the effect of different heat flux on the flow profiles during nucleate boiling at high mass flux, Figures 8, 9, and 10 plot high-speed image sequences for a mass velocity of G = 1038 kg/m^{2}s, P_{in} = 344 kPa, and ΔT_{sub} = 3.96 K at three different wall heat flux conditions, q" of 27.7%, 57.6%, and 94.1% q''_{CHF}, respectively. Again, the images in each sequence are 10 ms apart. At 27.7% q''_{CHF}, as shown in Figure 8, a great number of small and discrete bubbles flow into the visualization section in a well distributed fashion. Due to intense inertia and turbulent mixing with the high mass velocity, bubbles are well scattered and do not merge until a farther axial location of the visualization section when compared to the transient flow sequence at lower mass velocities in Figure 5. Near the outlet at the downstream of the visualization section, bubbles coalesce to form elongated vapor structures or plugs. At higher heat flux percentages of 57.6% and 94.1% q''_{CHF}, as shown in Figure 9 and Figure 10, due to the increased vapor generation leading to higher vapor velocities, liquid is spread outward covering the entire perimeter of the visualization tube. In the vapor core, among the fast-flowing vapor, entrained liquid strips are intermittently observed as thin linings with darker colors in the center of the tube.

D. Flow Visualization as a Function of Mass Flux and Heat Flux

Figure 11 shows flow patterns along the boiling curve for operating conditions of G = 561 kg/m^{2}s, P_{in} = 344 kPa, and ΔT_{sub} = 1.68 K, a low mass flux. Equilibrium quality values are shown on the left hand side of the plot and % of heat flux relate to the critical flux shown on the right hand side of the plot. For the heat flux of 5% q''_{CHF}, the wall superheat surpasses the required superheat for bubble nucleation, evidenced by bubble formation along the heated test section. Due to the small surface tension of cryogens, nucleated bubbles easily detach from the heated wall despite the small size. Departed bubbles then migrate towards the top surface with the aid of the body force. The resulting flow pattern is bubbly flow having numerous small sized bubbles concentrated near the top surface. With a slight increase of heat flux up to 7% q''_{CHF}, the bubbles become larger due to higher wall superheat, activating a greater number of nucleation sites on the heated wall. Departed bubbles effectively coalesce each other while traveling, resulting in larger and longer bubbles, as captured in the recording.

At 10% q''_{CHF}, aggressively nucleated and departed bubbles coalesce to form elongated vapor structures with an unstable wavy liquid-vapor interface flowing near the top wall, typical of plug flow. Notice numerous small grain-like bubbles flowing under the vapor structure that merge into the vapor stream atop. Further increasing the

heat flux up to 13% q''_{CHF}, vapor plugs become thicker due to an enhanced vapor production rate and coalescence to form even longer plugs.

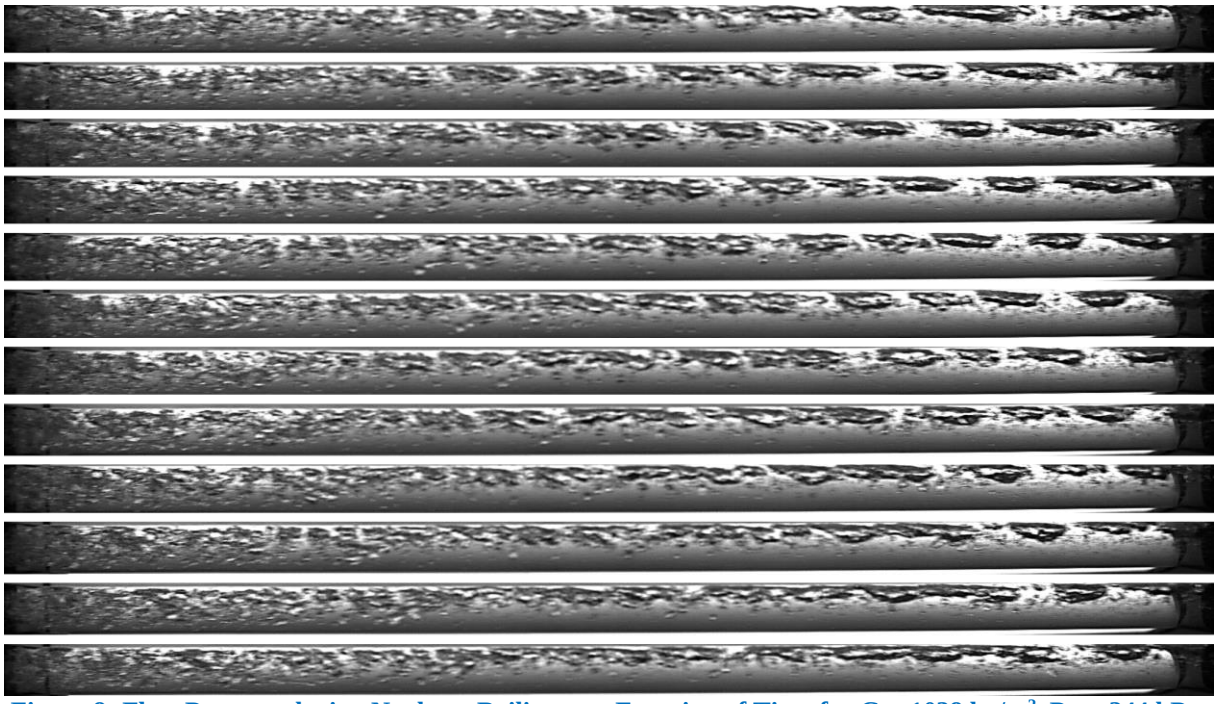

Figure 8: Flow Patterns during Nucleate Boiling as a Function of Time for G = 1038 kg/m^2, P_{in} = 344 kPa, $\Delta T_{sub,in}$ = 4 K, 27% q"$_{CHF}$, $x_{E,out}$ = 0

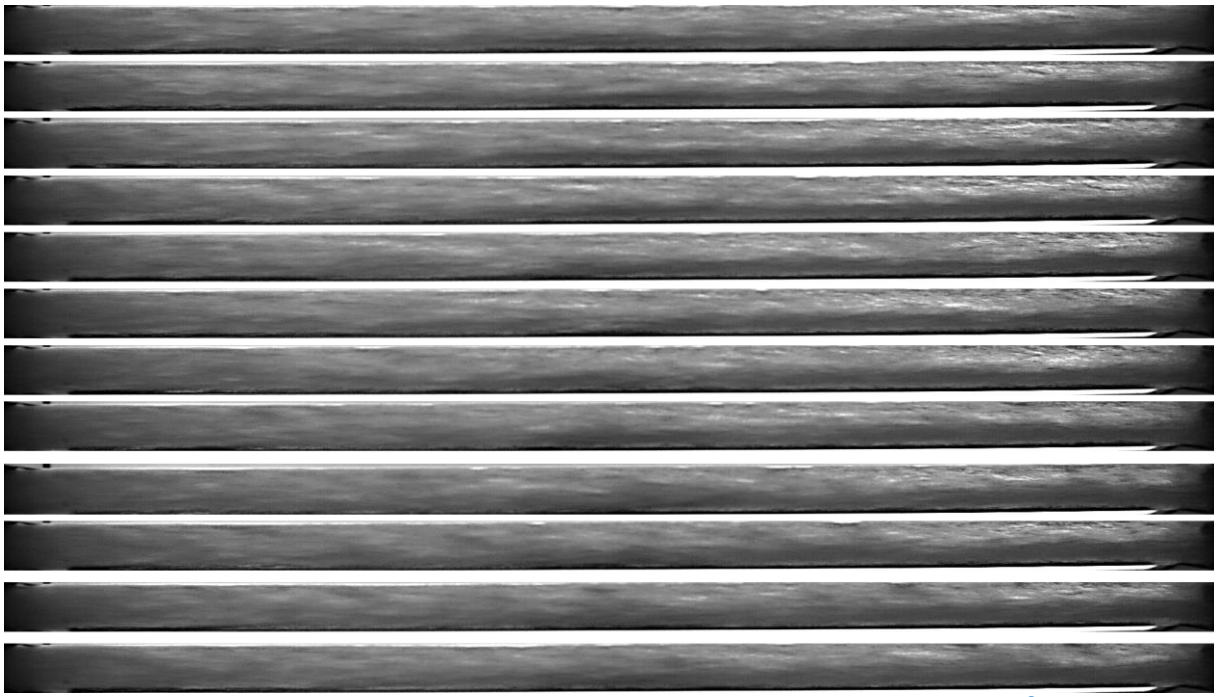

Figure 9: Flow Patterns during Nucleate Boiling as a Function of Time for G = 1038 kg/m^2, P_{in} = 344 kPa, $\Delta T_{sub,in}$ = 4 K, 57% q"$_{CHF}$, $x_{E,out}$ = 0.06

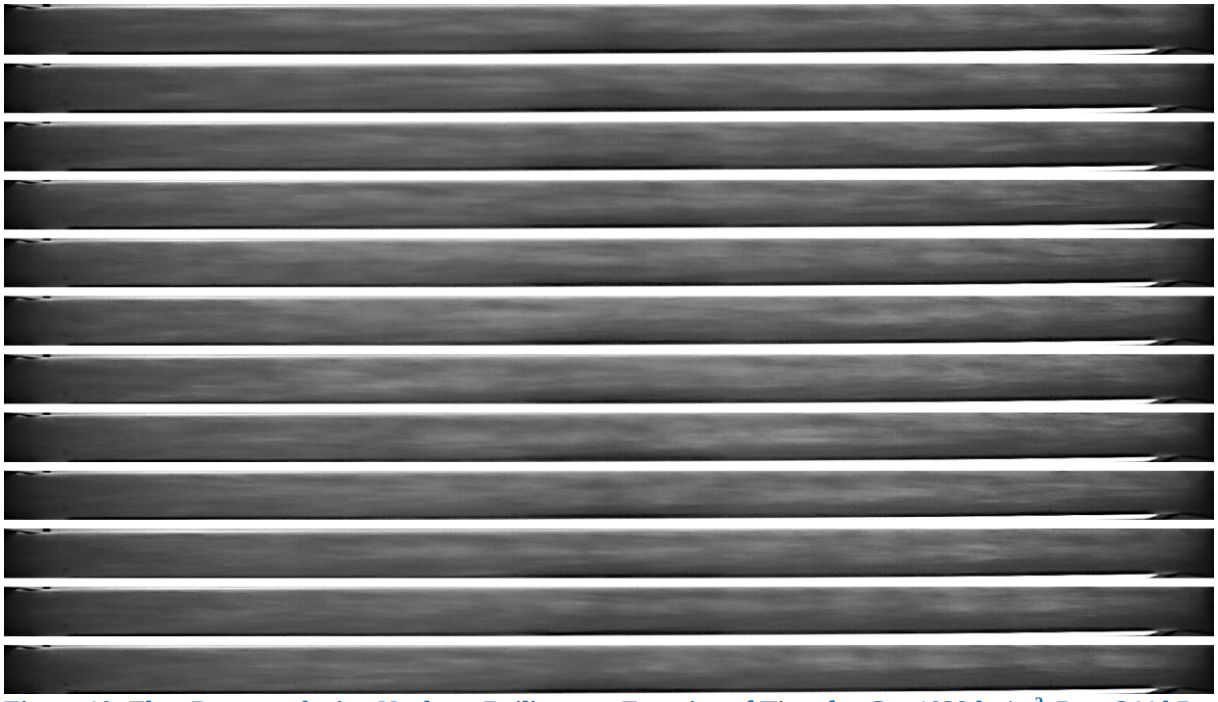

Figure 10: Flow Patterns during Nucleate Boiling as a Function of Time for G = 1038 kg/m^2, P_{in} = 344 kPa, $\Delta T_{sub,in}$ = 4 K, 94% q"$_{CHF}$, $x_{E,out}$ = 0.12

At 19%–34% q''_{CHF}, aggressive coalescence takes place to produce a continuous vapor film structure spanning almost the entire visualization section length, causing vapor stratification. However, note that the flow pattern is not perfect stratified flow having the top surface entirely covered by vapor film. Instead, the flow pattern shows a very thin layer of liquid persisting on top of the vapor structure. Due to high vapor velocity, liquid flowing under the vapor structure is dragged up and around the periphery, forming a thin layer of liquid fully wetting the tube. This flow pattern is called stratified annular flow as was identified and explained by Van Dresar et al. [19] whose experiments were focused on the lower mass velocity range rather than that of the current study.

At a heat flux of 59% q''_{CHF}, the annulus liquid layer becomes thinner, and the vapor core grows thicker with increasing heat flux. As the vapor volume fraction increases, due to further fluid acceleration, flow stratification gradually fades away resulting in a relatively symmetric flow structure. At 59% q''_{CHF} until CHF, due to the low h_{fg}, the required wall superheat for cryogens is lower than that of room temperature fluids. This unique characteristic of cryogens enables persistent bubble nucleation even within the annular liquid film which does not stop even at higher wall heat flux. Proving the suggested explanation, numerous small bubbles in the annular liquid film can be commonly observed in the heat flux range from 34% q''_{CHF} until CHF in Figure 11, where the flow patterns are annular. At 79% q''_{CHF}, a uniform annular liquid layer thickness can be observed along with a thicker and faster vapor core. Very near CHF, the liquid layer thickness remarkably attenuates, especially near the top surface, increasing the chances of the top liquid layer being partially dried out. The partially dried out surface within the test section, which is then continuously exposed to a vapor-only environment lacking latent heat transfer, experiences a sudden increase of wall temperature excursion—in other words, CHF.

Figure 12 depicts flow patterns along the boiling curve for operating conditions of G = 700 kg/m^{2}s, P_{in} = 344 kPa, and ΔT_{sub} = 2.86 K, an intermediate mass flux. Mass velocity is notably higher than the cases depicted in Figure 11, yet a similar flow pattern progression until CHF is observed except for the following differences. With similar heat flux percentage, vapor bubble size is much smaller at higher mass flux. Due to higher flow inertia under the higher mass velocity condition, departed small bubbles are rapidly flushed away without having a chance to merge with neighboring bubbles to form larger vapor structures. Accordingly, at a higher mass velocity, it requires greater wall heat flux to reach annular flow. Notice the enhanced CHF value at higher G, almost double the CHF at lower G.

Figure 13 shows flow patterns along the boiling curve for operating conditions of G = 1038 kg/m^{2}s, P_{in} = 344 kPa, and ΔT_{sub} = 3.96 K, a high mass flux. Notice the CHF value is nearly constant regardless of the magnitude of mass flux from Figure 12 to 13. Even in the highest mass flux condition, similar flow patterns and regime

transitions continue, but at higher heat flux percentages due to rapid vapor removal, which effectively disturbs bubble coalescence when compared to lower mass velocity conditions. Nevertheless, flow patterns near or at CHF in all the cases are patterns of annular flow with thin liquid annular film and vapor at the core. Notice the gradual thinning of both the bottom and top liquid layer thickness with heat flux percentage from 44% to 100 % q''_{CHF} based on which CHF is triggered by partial dry-out of either top or bottom liquid film.

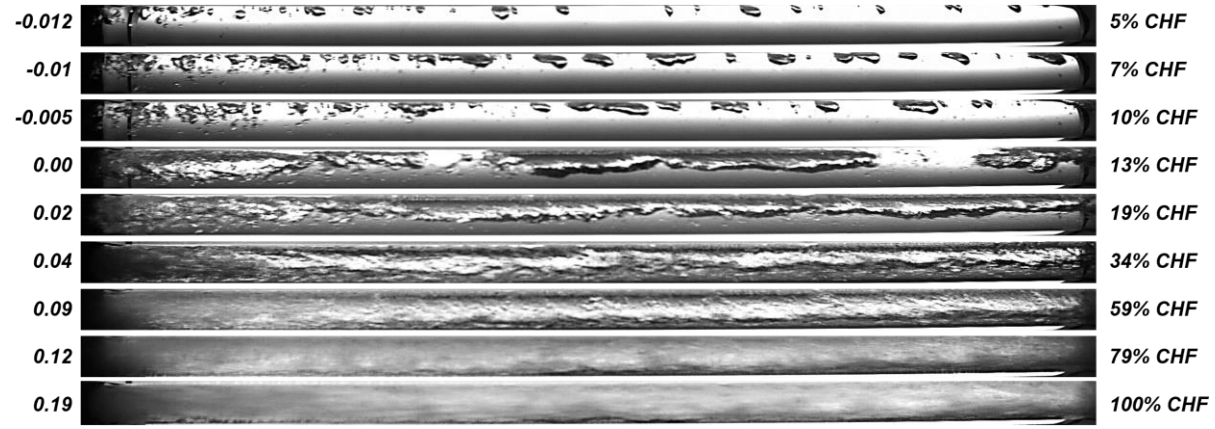

Figure 11: Flow Patterns during Nucleate Boiling at Different Heat Fluxes for G = 561 kg/m^2, P_{in} = 344 kPa, $\Delta T_{sub,in}$ = 1.7 K, CHF = 56.59 kW/m^2

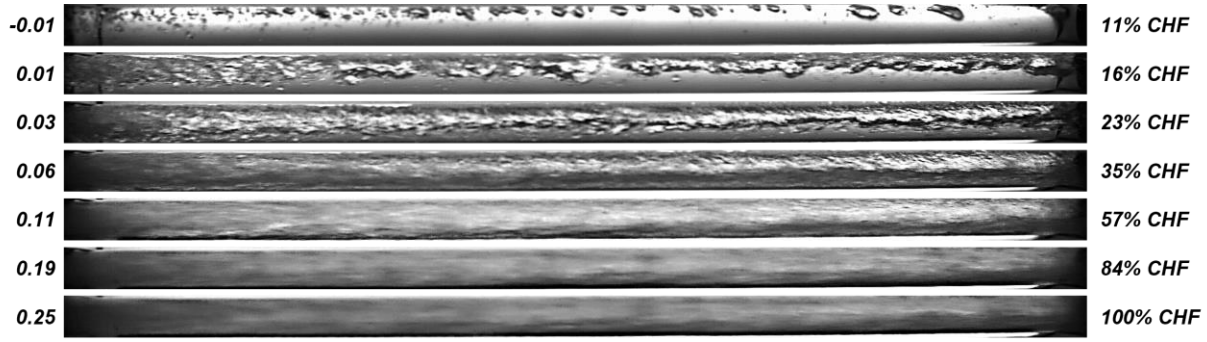

Figure 12: Flow Patterns during Nucleate Boiling at Different Heat Fluxes for G = 700 kg/m^{2}s, P_{in} = 344 kPa, $\Delta T_{sub,in}$ = 2.9 K, CHF = 99.25 kW/m^2

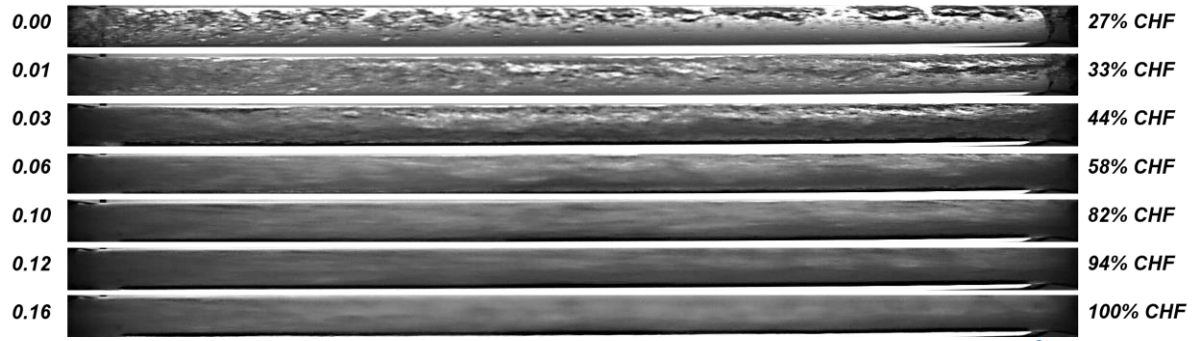

Figure 13: Flow Patterns during Nucleate Boiling at Different Heat Fluxes for G = 1038 kg/m^{2}s, P_{in} = 344 kPa, $\Delta T_{sub,in}$ = 3.9 K, CHF = 100.2 kW/m^2

V. Conclusions

This paper presented a summary of recent steady state liquid nitrogen flow boiling experiments conducted in the horizontal flow configuration in terrestrial gravity to understand how heat flux and mass flux impact liquid nitrogen flow boiling flow patterns. Tests were conducted over a wide range of flow directions, mass flux, heat flux, inlet subcooling, and equilibrium quality. A summary of results is provided for cryogenic nucleate flow boiling heat transfer and visualization in the horizontal flow configuration:

1. Nucleate boiling heat transfer coefficients increase with increasing heat flux. At low heat flux, there is a sharper rise in HTC due to the efficiency of nucleate boiling heat transfer. As heat flux approaches the critical heat flux, the HTC levels off due to suppression of nucleate boiling.
2. Nucleate boiling HTC increases with increasing mass flux. This trend is noticeable at low mass flux, but levels off at high mass flux due to inertial forces dominating over buoyancy forces.
3. Multiple two-phase flow regimes are observed: bubbly flow, plug flow, slug flow, stratified annular flow, and annular flow.
4. Flow regime transitions are observed with increasing heat flux facilitated by bubble growth, departure, and coalescence, resulting in regime developments from small discrete bubbles into larger and oblong vapor structures, in other words, plug flow.
5. Further flow regime transitions are observed from plug flow to stratified annular with further increase of heat flux, revealing the effect of body force on two-phase flow structures.
6. Further increase of heat flux near CHF leads to regime transition into annular flow with no flow stratification brought by significantly increased flow velocity at high fluid quality.
7. Increased mass velocity aids in attenuating the body force effect on two-phase flow structures, resulting in less or no flow stratification at high mass velocity conditions.

As stated, the new Purdue cryogenic flow boiling facility has successfully filled several gaps in the world consolidated cryogenic flow boiling database. Particularly noteworthy is the contribution of new high-speed flow visualization imagery and detailed descriptions of the ensuing flow profiles as a function of operating parameters, considering the near-complete lack of cryogenic flow boiling visualization reported in the literature. The rig can be used to further investigate the effect of other operating parameters on cryogenic flow boiling, including operating pressure, inlet subcooling, etc.

References

[1] Morehead, R.L., Melcher, J.C., Atwell, M.J., Hurlbert, E.A., Desai, P.S., Werlink, R., "Vehicle-Level Oxygen/Methane Propulsion System Hotfire Demonstration at Thermal Vacuum Conditions" *AIAA-2017-4748, 2017 Joint Propulsion System*, Atlanta, GA, July 10 – 12. 2017.

[2] Chandler, F., Bienhoff, D., Cronick, J., and Grayson, G. "Propellant Depots for Earth Orbit and Lunar Exploration" *AIAA-2007-6081*, SPACE Conference, Long Beach, CA, September 18 – 20, 2007.

[3] Meyer, M., Hartwig, J.W., Sutherlin, S., and Colozza, A. "Recent Concept Study for Cryogenic Fluid Management to Support Opposition Class Crewed Missions to Mars" *Cryogenics* 129, 103622. 2022.

[4] Oleson, S. R., et al. "Compass Final Report: Nuclear Electric Propulsion (NEP)-Chemical Vehicle 1.2" *NASA-TM-202100017131*, September, 2021.

[5] Hartwig, J.W., Hu, H., Styborski, J., and Chung, J. "Comparison of Cryogenic Flow Boiling in Liquid Nitrogen and Liquid Hydrogen" *International Journal of Heat and Mass Transfer* Volume 88, 662 – 673. 2015.

[6] Ganesan, V., Patel, R., Hartwig, J.W., and Mudawar, I. "Review of Databases and Correlations for Saturated Flow Boiling Heat Transfer Coefficient for Cryogens in Uniformly Heated Tubes, and Development of New Consolidated Database and Universal Correlations" *International Journal of Heat and Mass Transfer* 179. 121656. 2021.

[7] Ganesan, V., Patel, R., Hartwig, J.W., and Mudawar, I. "Universal Critical Heat Flux (CHF) Correlations for Cryogenic Flow Boiling in Uniformly Heated Tubes" *International Journal of Heat and Mass Transfer* 166, 120678. 2021.

[8] Ganesan, V., Patel, R., Hartwig, J.W., and Mudawar, I. "Universal Correlations for Post-CHF Saturated and Superheated Flow Film Boiling Heat Transfer Coefficient, Minimum Heat Flux and Rewet Temperature for

Cryogenic Fluids in Uniformly Heated Tubes" *International Journal of Heat and Mass Transfer* 195, 123054. 2022.
[9] Ganesan, V., Patel, R., Hartwig, J.W., and Mudawar, I. "Development of Two-Phase Frictional Pressure Gradient Correlation for Saturated Cryogenic Flow Boiling in Uniformly Heated Tubes" *International Journal of Heat and Mass Transfer* 220, 124901. 2024.
[10] Kim, S., Foster, D., Damle, N., Mudawar, I., and Hartwig, J.W. "Experimental Investigation of Flow Orientation Effects on Cryogenic Flow Boiling" *International Journal of Heat and Mass Transfer* 220, 124940. 2024.
[11] Kim, S., Damle, N., Mudawar, I., and Hartwig, J.W. "Experimental Heat Transfer Results and Flow Visualization of Horizontal Near-Saturated Liquid Nitrogen Flow Boiling in Uniformly Heated Circular Tube Under Earth Gravity" *Applied Thermal Engineering* 246. 122934. 2024.
[12] Velat, C. "Experiments in Cryogenic Two Phase Flow" *Masters Thesis*, University of Florida, 2004.
[13] Kawanami, O., Nishida, T., Honda, I. Kawashima, Y., Ohta, H. "Flow and Heat Transfer on Cryogenic Flow Boiling during Tube Quenching under Upward and Downward Flow" *Microgravity Science and Technology* 19, 137–138. 2007a.
[14] Kawanami, O., Azuma, H., and Ohta, H. "Effect of Gravity on Cryogenic Boiling Heat Transfer during Tube Quenching" *International Journal of Heat and Mass Transfer* 50, 3490–3497. 2007.
[15] Yuan, K., Ji, Y., Chung, J., and Shyy, W. "Cryogenic Boiling and Two-Phase Flow during Pipe Chilldown in Earth and Reduced Gravity" *Journal of Low Temperature Physics* 150, 101–122. 2008.
[16] Rame, E., Hartwig, J.W., and McQuillen, J.B. "Flow Visualization of Liquid Hydrogen Line Chill Down Tests" *AIAA-2014-1074, 2014 AIAA SciTech Conference*, National Harbor, MD, January 13 – 17, 2014.
[17] Hartwig, J.W., Styborski, J., Stiegemeier, B., Chung, J.N., Rame, E., and McQuillen, J.B., "Liquid Hydrogen Transfer Line Chilldown Experiments. II. Analysis" *International Journal of Heat and Mass Transfer* 156, 119805, 2020.
[18] Simoneau, R.J. and Simon, F.F. "A Visual Study of Velocity and Buoyancy Effects on Boiling Nitrogen" *NASA-TN-D-3354*, 1966.
[19] Van Dresar, N.T., Siegwarth, J.D., and Hasan, M.M. "Convective Heat Transfer Coefficients for Near-Horizontal Two-Phase Flow of Nitrogen and Hydrogen at Low Mass and Heat Flux" *Cryogenics* 41, 805-811. 2001.
[20] Fu, X., Qi, S., Zhang, P., and Wang, R. "Visualization of Flow Boiling of Liquid Nitrogen in a Vertical Mini-Tube" *International Journal of Multiphase Flow* 34, 333–351. 2008.
[21] Sharma, S.L., Hibiki, T., Ishii, M., Brooks, C.S., Schlegel, J.P., Liu, Y., Buchanan, J.R., Turbulence-induced bubble collision force modeling and validation in adiabatic two-phase flow using CFD, Nucl Eng and Design 312, 399–409. 2017.